Sn@CNT Nanostructures Rooted in Graphene with High and Fast Li-Storage Capacities

Yuqin Zou and Yong Wang*

Department of Chemical Engineering, School of Environmental and Chemical Engineering, Shanghai University, Shangda Road 99, Shanghai 200444, People's Republic of China

ABSTRACT Development of materials with carefully crafted nanostructures has been an important strategy for the next-generation lithium-ion batteries to achieve higher capacity, longer cycle life, and better rate capability. Graphene-based and Sn-based anode materials are promising anodes with higher capacities than graphite; however, most of them exhibit fast capacity fading at prolonged cycling and poor rate capability. This paper reports a hierarchical Sn@CNT nanostructure rooted in graphene, which exhibits larger than theoretical reversible capacities of 1160−982 mAh/g in 100 cycles at 100 mA/g and excellent rate capability (828 mAh/g at 1000 mA/g and 594 mAh/g at 5000 mA/g). The excellent electrochemical performances compared to graphene/Sn-based anodes have been attributed to the efficient prevention of graphene agglomeration by Sn@CNT decoration and the increased electrochemical activities of Sn by CNT shell protection and GNS support.

KEYWORDS: carbon nanotube · graphene · lithium ion batteries · Sn · SnS_2

With rising energy costs, today's society is searching for clean and renewable sources to meet energy needs. Graphene and carbon nanotubes (CNTs) are intriguing components of a new class of carbon materials owing to their unique physical, chemical, and mechanical properties.[1−3] Since its discovery in 2004,[4] graphene-based materials have been suggested as promising electrode materials for energy-related devices such as lithium-ion batteries, supercapacitors, and solar cells.[5−22] However, one inherent key problem is its prone aggregation after removing the solvent in practical applications.[2,3] The reassembly of graphene into graphite sheets could take place due to intersheet van der Waals attraction, leading to no largely different properties than common graphite. For example, graphene nanosheets (GNSs) showed substantially enhanced Li-storage capacities (∼500−1100 mAh/g) in initial cycles than commercial graphite anodes (theoretical value: 372 mAh/g). However, they displayed fast capacity fading upon prolonged cycling and poor rate performances.[5−10]

Functional nanocomposite materials are formed by reinforcing two or more materials of varying merits, and these components work synergistically to deliver complementary performances.[23,24] Recently, carbonaceous materials have been used as matrices to be composited with SnS_2.[25,26] The electrochemical performances were greatly improved compared to bare SnS_2 because carbons could absorb the mechanical failure induced by volume change (up to ∼300%) during the lithium reaction with Sn and hinder the agglomeration of SnS_2 particles. In the absence of carbon, SnS_2 materials, while impressive for a high theoretical capacity of 645 mAh/g, usually displayed poor cycle life.[27−31] Owing to excellent electrical conductivity, mechanical strength, high flexibility, and high specific surface area, graphene or CNTs can also be a promising compositing matrix.[11−22] On the other hand, it is believed that carefully crafted growth of a Sn-based nanostructure on graphene may be helpful for keeping graphene nanosheets separated, thereby preserving their unique properties upon repetitive cycling.

Herein, we demonstrate a unique graphene−Sn@CNT nanostructure with highly reversible large Li-storage capacities and excellent rate performances as anodes for Li-ion batteries. The composite was derived from the graphene−SnS_2 nanocomposite, which also showed improved electrochemical performances.

RESULTS AND DISCUSSION

Powder X-ray diffraction patterns of bare SnS_2, GO, GNS−SnS_2, and GNS−Sn@CNT are shown in Figure 1a. The (002) peak of graphite was observed at 23.7° for GNS−SnS_2. The corresponding interlayer spacing was 0.374 nm, which was slightly larger than the standard graphite (∼0.335 nm). A few other peaks in the GNS−SnS_2 composites could be indexed into SnS_2 materials (PDF: 23-0677). For the GNS−Sn@CNT composites, a wide (002) peak was observed at 24.2° with the

* Address correspondence to yongwang@shu.edu.cn.

Received for review July 19, 2011 and accepted September 22, 2011.

Published online September 22, 2011
10.1021/nn2027159

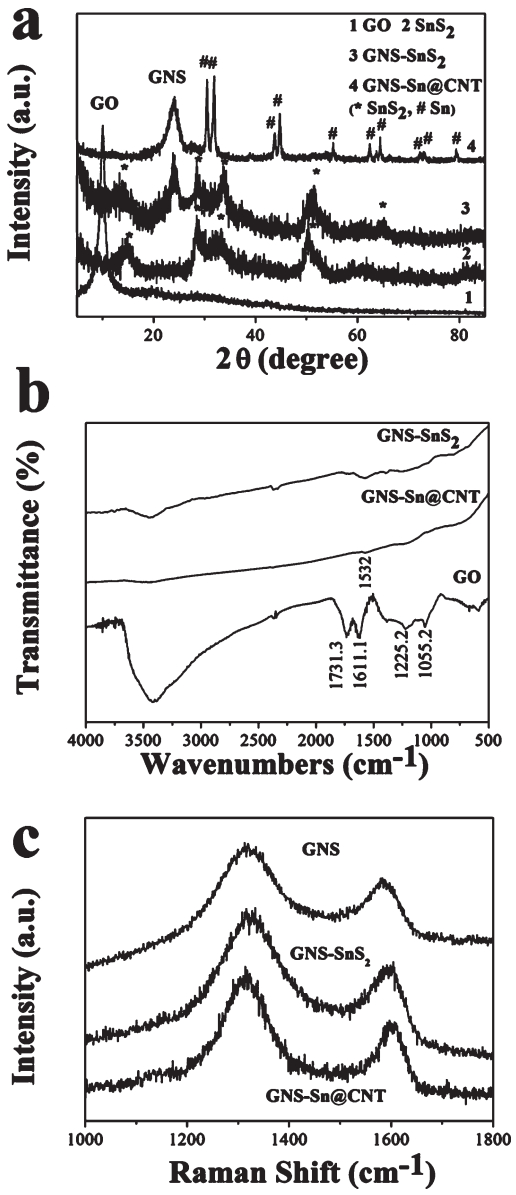

Figure 1. (a) Powder X-ray diffraction (XRD) patterns of the products. (b) FTIR spectra of GO, GNS−SnS_2, and GNS−Sn@CNT. (c) Raman spectra of GNS, GNS−SnS_2, and GNS−Sn@CNT.

interlayer spacing of 0.367 nm. This peak should be ascribed to the conjunct effect of CNT and graphene nanosheets. The other peaks were in accordance with the Sn metal (PDF: 04-0673). The characteristic peaks were not found for S-based materials in the GNS−Sn@CNT because SnS_2 was reduced by C_2H_2 to Sn and CS_2. The CS_2 with a low boiling point of 46 °C was evaporated in the high-temperature (550 °C) growth process. The FTIR spectra of GO, GNS−SnS_2, and GNS−Sn@CNT are shown in Figure 1b. For graphene oxide, the peak at 3411 cm^{-1} was attributed to the O−H stretching vibration of adsorbed water molecules and surface OH groups. A few stretches of 1731 and 1225 cm^{-1} could be attributed to the presence of abundant O═C and O−C functional groups on the GO

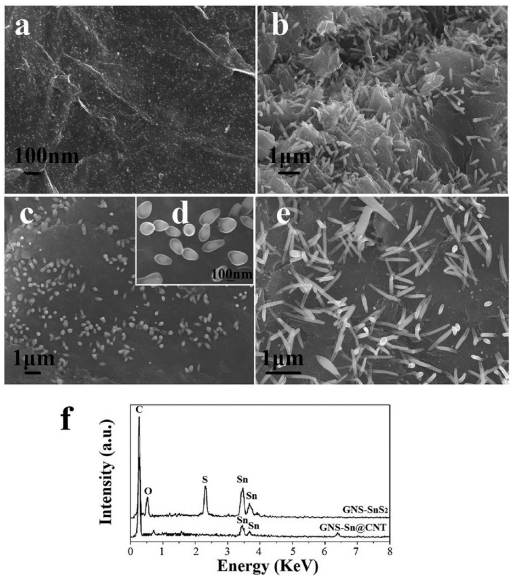

Figure 2. SEM images of (a) GNS-supported SnS_2 nanoparticles, (b) GNS−Sn@CNT, (c,d) GNS−Sn@C particles after reduced reaction time of 15 min, (e) GNS−Sn@CNT after prolonged reaction time of 3 h. (f) EDS patterns of GNS−SnS_2 and GNS−Sn@CNT.

surface.[22] After a thermal reduction, these O-containing functional groups derived from the intensive oxidation were not present in the GNS−SnS_2 and GNS−Sn@CNT composites, reflecting that graphene oxide has been reduced to graphene nanosheets. For two GNS-based composites, a new small stretch appeared at ~1532 cm^{-1}, which could be ascribed to the skeletal vibration of graphene sheets.[22] The Raman spectra of GNS, GNS−SnS_2, and GNS-Sn@CNT are shown in Figure 1c. The *D*/*G* intensity ratios of GNS, GNS−SnS_2, and GNS−Sn@CNT were 1.21, 1.29, and 1.50, respectively. The more disordered structure of GNS-based composites may be due to the partial insertion of SnS_2 or Sn@CNT into GNS. This may facilitate the lithium diffusion and enhance storage capacity in the composites.[24]

Figure 2 and Supporting Information Figure S1 show the SEM images of SnS_2, graphene nanosheets (GNSs), GNS−SnS_2, and GNS−Sn@CNT nanocomposites. Pristine SnS_2 nanoparticles were heavily aggregated (Supporting Information, Figure S1). In the presence of GNS, SnS_2 (melting point = 600 °C) nanoparticles were separated well and distributed uniformly on GNS (Figure 2a). Their particle sizes were around 5−10 nm in the composite. For the GNS−Sn@CNT composite, a large number of rod-like nanostructures were rooted in GNS (Figure 2b). Their lengths were ~0.6−1.2 μm. To examine the initial growth stage of Sn@CNT growth, reaction time was reduced to 15 min. A few Sn@C core−shell particles around 150 nm in size were observed (Figure 2c,d), indicating that C_2H_2 may be decomposed around Sn (melting point = 232 °C) droplet catalysts in the growth process at 550 °C. The Sn@CNT lengths could be slightly enlengthed to

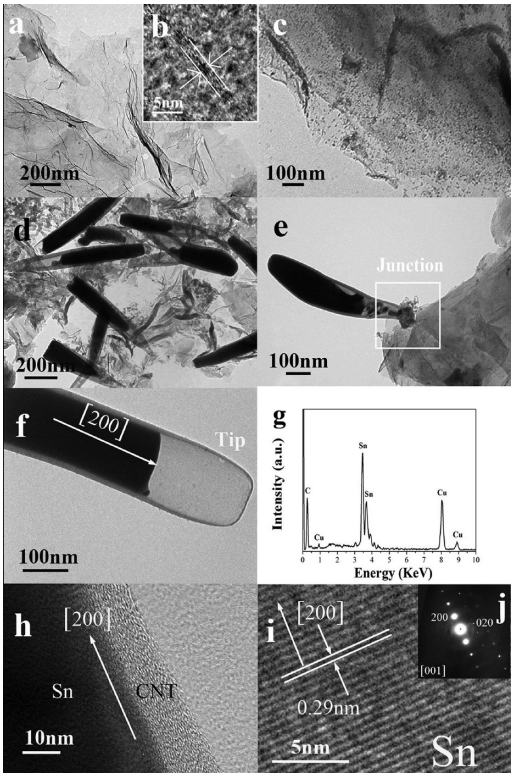

Figure 3. (a) TEM image of GNS, the inset is (b) the HRTEM image showing the cross section of GNS, (c) GNS-supported SnS_2 nanoparticles. (d–f) TEM images of GNS–Sn@CNT. (g) EDS pattern. (h) HRTEM image showing the carbon shell. (i) HRTEM image showing the Sn core. (j) SAED pattern showing the single-crystalline Sn structure.

~0.7–1.5 μm (Figure 2e) after prolonged reaction of 3 h. The energy-dispersive X-ray spectroscopy (EDS) results of GNS–SnS_2 and GNS–Sn@CNT are shown in Figure 2f. A few elements such as C, O, S, and Sn were present in GNS–SnS_2. The S element disappeared in the GNS–Sn@CNT because SnS_2 was reduced by C_2H_2 to Sn and the resulting CS_2 could be evaporated in the high-temperature reaction system. This is in good agreement with the XRD pattern. The elemental results were confirmed by a carbon–sulfur analyzer, and the carbon contents were determined to be 46.5% in GNS–SnS_2 and 65.8% in GNS–Sn@CNT. The CNT was calculated to be 20.2% in the GNS–Sn@CNT composite assuming there was no weight loss of Sn and GNS in the CVD reaction of GNS–SnS_2 to GNS–Sn@CNT.

Figure 3 shows the TEM images of GNS, GNS–SnS_2 nanoparticles, and the GNS–Sn@CNT nanocomposite. GNSs were quite thin under electron imaging (TEM image in Figure 3a and SEM image in Supporting Information, Figure S1), and the thickness of GNS was determined to be ~1.8 nm by the inset HRTEM image of Figure 3b. The calculated carbon layers were only ~5 layers. Figure 3c confirmed that 5–10 nm SnS_2 nanoparticles were uniformly dispersed on GNS without detectable particle agglomeration. The GNS–Sn@CNT composite is shown in the TEM images of Figure 3d–f. Interestingly, those rod-like structures shown in the SEM image of Figure 2b indeed had core–shell nanostructures. The uniform CNT shell was ~6–10 nm in thickness. The inner black filler cores were Sn nanorods (~150 nm in diameter), and no Sn materials were found on the exterior CNT walls. Figure 3e shows the junction of Sn@CNT and GNS, which reveals that the carbon materials in the junction were tightly integrated. The corresponding EDS pattern in Figure 3g confirmed the presence of Sn materials in the Sn@CNT nanostructure. The HRTEM image in Figure 3h shows that the carbon nanotube overlayer was made up of staggered and shortened graphene sheets, which could provide multichannels for lithium insertion and extraction.[20,24] A lattice image of the filled Sn nanorod is shown in the HRTEM image of Figure 3i. The (200) crystal plane of Sn tetragonal structure could be identified by a clear observation of the interplanar distance of ~0.29 nm. Each Sn nanorod was single crystalline as shown in the selected area electron diffraction (SAED) pattern in Figure 3j. The growth direction of the Sn nanorod was along the [200] direction.

On the basis of the above observations, SnS_2 nanoparticles were converted to the novel Sn@CNT nanostructure on the GNS substrate by a chemical vapor deposition technique in this study. The growth mechanism of Sn@CNT on GNS may be proposed below: SnS_2 was first reduced by C_2H_2 to Sn and CS_2. The CS_2 with a low boiling point of 46 °C was evaporated in the tube furnace with the carrier gas. The resulting melt Sn materials (melting point = 232 °C, boiling point = 2602 °C) were mobile on the GNS substrate at the reaction temperature (550 °C). The aggregated Sn droplet was the catalyst formed *in situ* to decompose C_2H_2 and promote continuing growth of CNTs. CNTs should grow following a "bottom growth" mechanism because experimentally there were no Sn catalysts on the CNT tips.[32,33] Concurrently, these mobile Sn droplets were infiltrated into the CNT cavities by the capillary force. The filled Sn materials exhibited nanorod morphologies because they were shaped by the hard template of CNT. The *in situ* growth of CNTs from the liquid pool of the filler and catalyst materials ensured a highly efficient encapsulation of Sn materials with nearly 100% filling structure yield. There was no filler materials observed on the exterior walls of CNTs (Figure 3e). The capillary effect has been widely used to fill CNTs with foreign materials; however, the previous CNT-encapsulated nanostructures were usually produced by immersing prefabricated CNTs in the solution containing filler precursors.[34,35] The filling structures were usually obtained at a low filling yield because CNTs have very small tip openings and a large aspect ratio. The filler materials were hard to be infiltrated completely into CNTs, and some filler materials were inevitably found on exterior CNT walls.[34,35] The

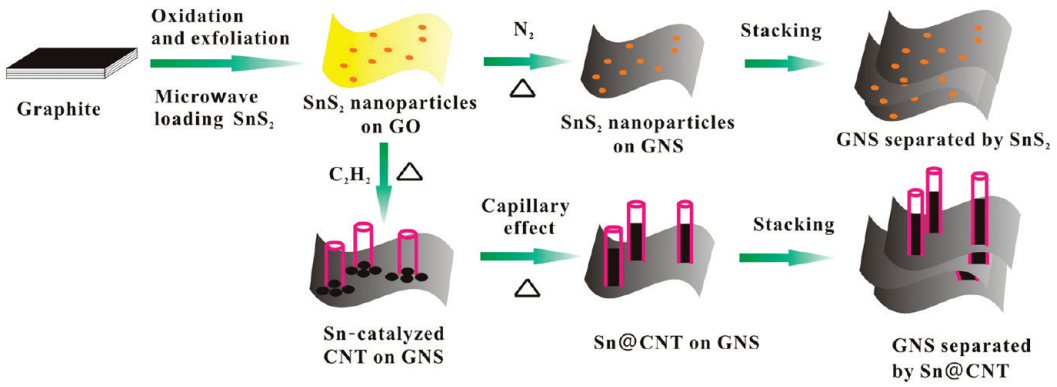

Figure 4. Schematic sketch of the growth process.

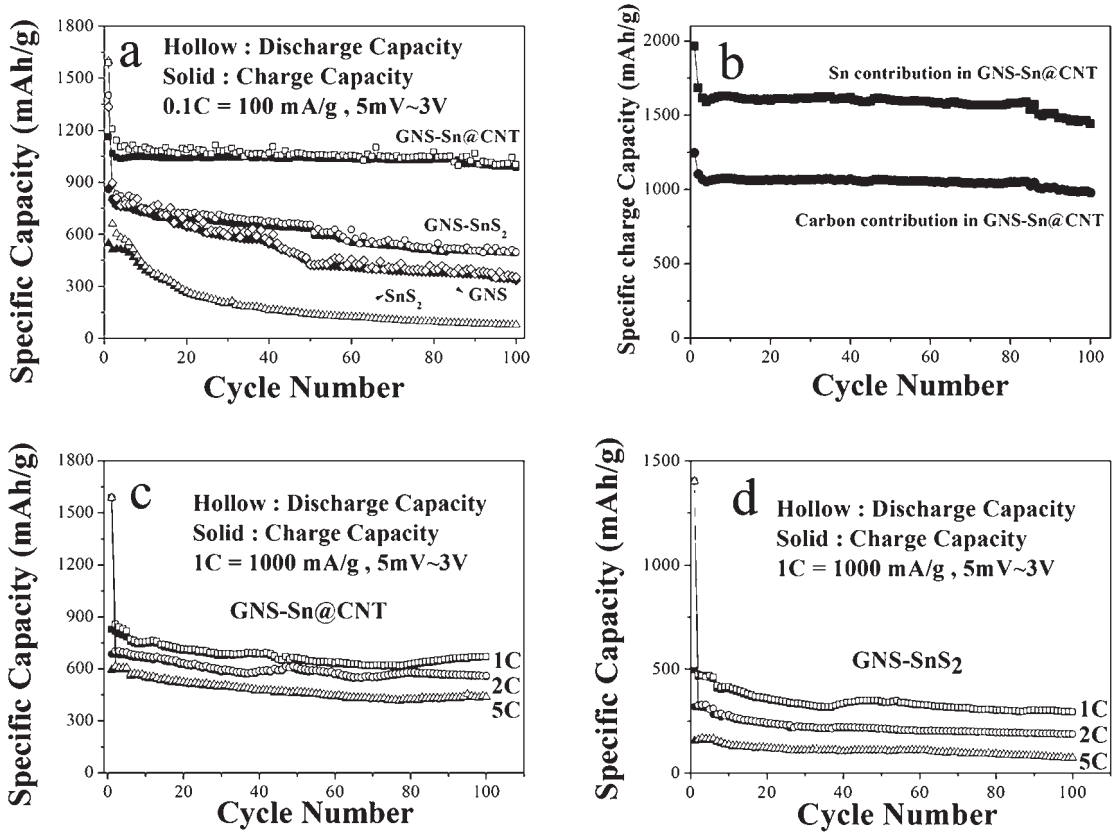

Figure 5. (a) Cycling performances of GNS, SnS_2, GNS−SnS_2, and GNS−Sn@CNT at 0.1C (1C = 1000 mA/g). (b) Sn contribution in GNS−Sn@CNT, assuming that carbon contributed a constant capacity of 744 mAh/g (the theoretical value of GNS). The charge capacity of Sn contribution was calculated as (composite capacity − 744 × weight fraction of carbon)/(weight fraction of Sn). The carbon contribution in GNS−Sn@CNT was calculated accordingly, assuming that Sn contributed a constant capacity of 992 mAh/g (the theoretical value of Sn). (c) Cycling performances of GNS−Sn@CNT at large current rates. (d) Cycling performances of GNS−SnS_2 nanoparticles at large current rates.

complete filling of Sn in CNTs could offer a better electrical contact and enhanced structure stability of Sn materials. The decoration of numerous Sn@CNT nanostructures on GNS could also help keep GNS separated against their reassembly. The growth process of GNS−SnS_2 nanoparticles and the GNS−Sn@CNT hierarchical nanostructure is sketched in the Figure 4.

Figure 5a and Supporting Information Figures S2 and S3 show the electrochemical properties of graphene nanosheets (GNSs), SnS_2, GNS−SnS_2, and GNS−Sn@CNT at a constant current of 100 mA/g (0.1C,1C = 1000 mA/g). The initial reversible charge capacities of GNS, SnS_2 particle, and GNS−SnS_2 were 863, 546, and 858 mAh/g, respectively. GNS−Sn@CNT exhibited a very large initial charge capacity of 1160 mAh/g. This capacity is much higher than the theoretical values of graphite (372 mAh/g), graphene (744 mAh/g), Sn (992 mAh/g), and previous bare graphene,[5−10] Sn−graphene,[11−16] and Sn−CNT composites.[18−20] It is believed that the superior capacity is largely ascribed to the unique

structure of the Sn@CNT grown on GNS. A large amount of micropores or defects in the disordered carbon should store an extra amount of lithium ions.[24] Despite a fast capacity fading, disordered GNS materials could exhibit an initial large reversible capacity of ~1050 mAh/g.[8] The reassembly of bare graphene to graphite may occur in previous unprotected graphene; however, this work uses the decoration of numerous Sn@CNT materials on the graphene surface to keep graphene nanosheets separated. The unique properties of few-layer graphene could be preserved upon repetitive Li-ion insertion and extraction. Therefore few-layer GNS in the GNS–Sn@CNT composite may exhibit larger Li-ion storage capacity than the agglomerated pristine GNS materials. Moreover, the presence of highly conductive GNS support and CNT skin around Sn may also facilitate the diffusion and storage of lithium ions in the Sn electrode. As measured by a four-electrode method, GNS–Sn@CNT exhibited an electrical conductivity of 28.1 s/cm, which is substantially higher than that of SnS_2 (3.2×10^{-5} s/cm), GNS–SnS_2 (1.2×10^{-3} s/cm), and GNS (5.1 s/cm). Lastly, the Li-ion storage has also been suggested by a possible faradaic capacitance[22] and absorption on both sides of graphene.[11,24] Figure 5a shows the cycling performances of SnS_2, GNS, GNS–SnS_2, and GNS–Sn@CNT at 0.1C (100 mA/g). A large reversible capacity of 982 mAh/g was retained for GNS–Sn@CNT after 100 cycles of discharge and charge. This value is still approaching the theoretical value of Sn (992 mAh/g) and larger than the simple weighted sum calculation based on carbonaceous materials (65.8 wt %) and Sn (34.2 wt %). By contrast, smaller capacities of ~400–650 mAh/g were obtained after 50–100 cycles for previous graphene–Sn composites.[11–16] To our knowledge, this large reversible capacity after 100 cycles has not been witnessed for bare graphene, pristine Sn, and Sn–C composite (C = CNT, graphene, and common carbonaceous materials) anode materials to date. Presented in another way, the capacity contribution from Sn or carbon during cycling in the GNS–Sn@CNT nanocomposite is shown in the Figure 5b. Either component exhibited very large higher than theoretical reversible capacities, assuming the other one contributed a constant theoretical capacity during cycling.

The GNS–SnS_2 composite exhibited a charge capacity of 493 mAh/g after 100 cycles. Notably, this retained reversible capacity was measured in a wide voltage window of 5 mV to 3 V. The upper limit voltages had to be restricted to ~1.1–1.3 V to achieve comparable cycle life in previous SnS_2-relative efforts.[27–31] Compared to the composites, bare GNS and SnS_2 nanoparticles exhibited much smaller charge capacities of 334 and 76 mAh/g, respectively, after 100 cycles. The rate performances of GNS–Sn@CNT and GNS–SnS_2 are shown in Figure 5c,d and Supporting Information, Figure S4. The GNS–Sn@CNT was cycled very well with high initial reversible capacities of 828, 686, and 594 mAh/g, respectively, at 1C, 2C, and 5C (1C = 1000 mA/g). In comparison, GNS–SnS_2 showed reduced reversible capacities with faster capacity fading at large currents. The excellent electrochemical performances of GNS–Sn@CNT at both low and large current rates should be ascribed to the following points: (1) the restacking of GNS to graphite is, in principle, hindered by the numerous CNTs decorated on the GNS surface, thereby preserving GNS unique properties in repetitive cycling process. (2) The robust and electrically conductive GNS substrate and flexible CNT skin around Sn materials prevents the aggregation of Sn and improves the electrical contact and integrity of the active electrode materials.[18,20] The Supporting Information Figure S5 shows the TEM images of the cycled electrode materials. The Sn@C nanostructure could still be observed clearly after 100 cycles in the presence of carbon black and binder materials. (3) The unique graphene–Sn@CNT nanostructure can facilitate the diffusion of the electrolyte, lithium ions, and electrons by offering a shortened diffusion pathway and large interface areas between electrolyte and electrode.[36–38] The porous space formed between lateral GNS and longitudinal CNTs in the stacked composite allows an easy diffusion of electrolyte and may be helpful to relieve the mechanical stress induced by a large volume change in lithium reactions with Sn materials. CNTs and GNS support are also useful for accommodating the electrode pulverization by a buffering effect.[11–20]

CONCLUSIONS

In summary, we prepared graphene–SnS_2 and novel graphene–Sn@CNT nanostructures in this work. The hierarchical graphene–Sn@CNT composite showed a distinctive synergetic effect when evaluated as an anode material for Li-ion batteries. It exhibited extraordinary large reversible capacities (1160–982 mAh/g in 100 cycles) and excellent high-rate performances. These outstanding electrochemical properties were ascribed to the efficient prevention of graphene agglomeration, increased electrical conductivity and mechanical stability, enhanced diffusion of lithium, electrolyte, and electron, and the buffering effect by CNT and GNS support.

METHODS

Preparation of Graphene Oxide (GO) and Graphene Nanosheets (GNSs). Graphene oxide (GO) was synthesized by chemical oxidation and exfoliation of natural graphite. Graphene nanosheets (GNS) were prepared by thermal reduction of graphene oxide. The details of preparation and material characterization of GNS and GO can be found in a previous publication.[17]

Preparation of GNS−SnS_2 and GNS−Sn@CNT. Ten milliliters of 0.3 M $SnCl_4 \cdot 5H_2O$ ethylene glycol solution was mixed with 10 mL of 0.6 M thiourea (CH_4N_2S) ethylene glycol solution to form a transparent solution. Then, 0.84 g of graphene oxide (GO) was ultrasonically dispersed in 40 mL of ethylene glycol for 30 min and then mixed with the above mixture solution. The suspension was transferred into a specialized glass tube and followed by microwave irradiation with continuous magnetic stirring in a single mode microwave reactor (Nova, EU Microwave Chemistry) at 180 °C for 20 min. The precipitates (GO−SnS_2) were collected, centrifuged, and washed with deionized water and ethanol before drying in a vacuum oven. The GO−SnS_2 products were heated in a tube furnace under flowing 80 sccm N_2 at 300 °C for 2 h to obtain GNS−SnS_2 nanoparticles.

The GO−SnS_2 nanoparticles were put in a tube furnace under flowing 80 sccm reactive gas mixture (5% C_2H_2 and 95% N_2). The CNT growth and *in situ* filling process was performed at 550 °C for 2 h. After cooling in pure N_2 to room temperature, GNS-supported carbon-nanotube-encapsulated Sn nanorods (GNS−Sn@CNT) were obtained.

Materials Characterizations. The obtained products were characterized by X-ray diffraction (XRD, Rigaku D/max-2550 V, Cu Kα radiation), field-emission scanning electron microscopy (FE-SEM, JSM-6700F) with an energy-dispersive X-ray spectrometer (EDS), and transmission electron microscopy/selected area electron diffraction/energy-dispersive X-ray spectroscopy (TEM/SAED/EDS, JEOL JEM-200CX and JEM-2010F) in the Instrumental Analysis and Research Center, Shanghai University. Raman spectroscopy was recorded on Renishaw in plus laser Raman spectrometer (excitation wavelength = 785 nm, excitation power = 3 mW, spot size = ~1.2 μm). Fourier transform infrared (FTIR) spectra were collected by a BIO-RAD FTS 135 FTIR spectrophotometer using the KBr pellet method. The electrical conductivity was measured by a four-electrode method using a conductivity detection meter (Shanghai Fortune Instrument, FZ-2010). The carbon and sulfur elements were measured by a high-frequency infrared carbon−sulfur analyzer (Keguo Instrument, HCS-500P).

Electrochemical Measurements. The working electrodes (~20 μm in thickness) were composed of 80 wt % of active material, 10 wt % of the conductivity agent (acetylene black), and 10 wt % of the binder (poly(vinylidene difluoride), PVDF, Aldrich). Lithium foil (China Energy Lithium Co., Ltd.) was used as counter and reference electrode. The electrolyte was 1 M $LiPF_6$ in a 50:50 w/w mixture of ethylene carbonate (EC) and diethyl carbonate (DEC). Electrochemical measurements were performed on a LAND-CT2001C test system. The Swagelok-type cells were discharged (lithium insertion) and charged (lithium extraction) at a constant current (100 mA/g, 0.1C,1C = 1000 mA/g) in the fixed voltage range of 5 mV to 3 V. Higher hourly rates (1, 2, or 5C) were also used, and the first cycle discharging was kept at 0.1C. Cyclic voltammetry was performed on a CHI660D electrochemical workstation at a scan rate of 0.1 mV/s.

Acknowledgment. The authors gratefully acknowledge the Instrumental and Analysis and Research Center, Shanghai University, for materials characterizations and the financial support from the Program for Professor of Special Appointment (Eastern Scholar), National Natural Science Foundation of China (50971085), and Shanghai Municipal Government (09JC140-6100, S30109).

Supporting Information Available: SEM and TEM images, cyclic voltammetry, initial discharge and charge curves of the products. This material is available free of charge *via* the Internet at http://pubs.acs.org.

REFERENCES AND NOTES

1. Bruce, P. G.; Scrosati, B.; Tarascon, J. M. Nanomaterials for Rechargeable Lithium Batteries. *Angew. Chem., Int. Ed.* **2008**, *47*, 2930–2946.
2. Chen, D.; Tang, L. H.; Li, J. H. Graphene-Based Materials in Electrochemistry. *Chem. Soc. Rev.* **2010**, *39*, 3157–3180.
3. Pumera, M. Graphene-Based Nanomaterials for Energy Storage. *Energy Environ. Sci.* **2011**, *4*, 668–674.
4. Novoselov, K. S.; Geim, A. K.; Morozov, S. V.; Jiang, D.; Zhang, Y.; Dubonos, S. V.; Grigorieva, I. V.; Firsov, A. A. Electric Field Effect in Atomically Thin Carbon Films. *Science* **2004**, *306*, 666–669.
5. Yoo, E. J.; Kim, J.; Hosono, E.; Zhou, H. S.; Kudo, T.; Honma, I. Large Reversible Li Storage of Graphene Nanosheet Families for Use in Rechargeable Lithium Ion Batteries. *Nano Lett.* **2008**, *8*, 2277–2282.
6. Wang, G. X.; Shen, X. P.; Yao, J.; Park, J. Graphene Nanosheets for Enhanced Lithium Storage in Lithium Ion Batteries. *Carbon* **2009**, *47*, 2049–2053.
7. Guo, P.; Song, H.; Chen, X. Electrochemical Performance of Graphene Nanosheets as Anode Material for Lithium-Ion Batteries. *Electrochem. Commun.* **2009**, *11*, 1320–1324.
8. Pan, D. Y.; Wang, S.; Zhao, B.; Wu, M. H.; Zhang, H. J.; Wang, Y.; Jiao, Z. Li Storage Properties of Disordered Graphene Nanosheets. *Chem. Mater.* **2009**, *21*, 3136–3142.
9. Wang, C. Y.; Li, D.; Too, C. O.; Wallace, G. G. Electrochemical Properties of Graphene Paper Electrodes Used in Lithium Batteries. *Chem. Mater.* **2009**, *21*, 2604–2606.
10. Yang, S. B.; Feng, X. L.; Zhi, L. J.; Cao, Q.; Maier, J.; Mullen, K. Nanographene-Constructed Hollow Carbon Spheres and Their Favorable Electroactivity with Respect to Lithium Storage. *Adv. Mater.* **2010**, *22*, 838–842.
11. Wang, G. X.; Wang, B.; Wang, X. L.; Park, J.; Dou, S. X.; Ahn, H.; Kim, K. Sn/Graphene Nanocomposite with 3D Architecture for Enhanced Reversible Lithium Storage in Lithium Ion Batteries. *J. Mater. Chem.* **2009**, *19*, 8378–8384.
12. Chen, Z. X.; Cao, Y. L.; Qian, J. F.; Ai, X. P.; Yang, H. X. Facile Synthesis and Stable Lithium Storage Performances of Sn-Sandwiched Nanoparticles as a High Capacity Anode Material for Rechargeable Li Batteries. *J. Mater. Chem.* **2010**, *20*, 7266–7271.
13. Zhang, M.; Lei, D.; Du, Z. F.; Yin, X. M.; Chen, L. B.; Li, Q. H.; Wang, Y. G.; Wang, T. H. Fast Synthesis of SnO_2/Graphene Composites by Reducing Graphene Oxide with Stannous Ions. *J. Mater. Chem.* **2011**, *21*, 1673–1676.
14. Zhang, L. S.; Jiang, L. Y.; Yan, H. J.; Wang, W. D.; Wang, W.; Song, W. G.; Guo, Y. G.; Wan, L. J. Mono Dispersed SnO_2 Nanoparticles on Both Sides of Single Layer Graphene Sheets as Anode Materials in Li-Ion Batteries. *J. Mater. Chem.* **2010**, *20*, 5462–5467.
15. Li, Y. M.; Lv, X. J.; Lu, J.; Li, J. H. Preparation of SnO_2-Nanocrystal/Graphene-Nanosheets Composites and Their Lithium Storage Ability. *J. Phys. Chem. C* **2010**, *114*, 21770–21774.
16. Kim, H.; Kim, S. W.; Park, Y. U.; Gwon, H.; Seo, D. H.; Kim, Y.; Kang, K. SnO_2/Graphene Composite with High Lithium Storage Capability for Lithium Rechargeable Batteries. *Nano Res.* **2010**, *3*, 813–821.
17. Chen, S. Q.; Wang, Y. Microwave-Assisted Synthesis of a Co_3O_4-Graphene Sheet-on-Sheet Nanocomposite as a Superior Anode Materials for Li-Ion Batteries. *J. Mater. Chem.* **2010**, *20*, 9735–9739.
18. Wang, Y.; Wu, M. H.; Jiao, Z.; Lee, J. Y. Sn@CNT and Sn@C@CNT Nanostructures for Superior Reversible Lithium Ion Storage. *Chem. Mater.* **2009**, *21*, 3210–3215.
19. Zhang, H. X.; Feng, C.; Zhai, Y. C.; Jiang, K. L.; Li, Q. Q.; Fan, S. S. Cross-Stacked Carbon Nanotube Sheets Uniformly Loaded with SnO_2 Nanoparticles: A Novel Binder-Free and High-Capacity Anode Material for Lithium-Ion Batteries. *Adv. Mater.* **2009**, *21*, 2299–2304.
20. Wang, Y.; Zeng, H. C.; Lee, J. Y. Highly Reversible Lithium Storage in Porous SnO_2 Nanotubes with Coaxially Grown Carbon Nanotube Overlayers. *Adv. Mater.* **2006**, *18*, 645–649.
21. Yang, S. B.; Feng, X. L.; Ivanovici, S.; Mullen, K. Fabrication of Graphene-Encapsulated Oxide Nanoparticles: Towards High-Performance Anode Materials for Lithium Storage. *Angew. Chem., Int. Ed.* **2010**, *49*, 8408–8411.
22. Murugan, A. V.; Muraliganth, T.; Manthiram, A. Rapid, Facile Microwave-Solvothermal Synthesis of Graphene Nanosheets

and Their Polyaniline Nanocomposites for Energy Storage. *Chem. Mater.* **2009**, *21*, 5004–5006.
23. Bai, H.; Li, C.; Shi, G. Q. Functional Composite Materials Based on Chemically Converted Graphene. *Adv. Mater.* **2011**, *23*, 1089–1115.
24. Kaskhedikar, N. A.; Maier, J. Lithium Storage in Carbon Nanostructures. *Adv. Mater.* **2009**, *21*, 2664–2680.
25. Li, Y.; Tu, J. P.; Huang, X. H.; Wu, H. M.; Yuan, Y. F. Net-like SnS/Carbon Nanocomposite Film Anode Material for Lithium Ion Batteries. *Electrochem. Commun.* **2007**, *9*, 49–53.
26. Kim, H. S.; Chung, Y. H.; Kang, S. H.; Sung, Y. E. Electrochemical Behavior of Carbon-Coated SnS_2 for Use as the Anode in Lithium-Ion Batteries. *Electrochim. Acta* **2009**, *54*, 3606–3610.
27. Brousse, T.; Lee, S. M.; Pasquereau, L.; Defives, D.; Schleich, D. M. Composite Negative Electrodes for Lithium Ion Cells. *Solid State Ionics* **1998**, *113−115*, 51–56.
28. Momma, T.; Shiraishi, N.; Yoshizawa, A.; Osaka, T.; Gedanken, A.; Zhu, J.; Sominski, L. SnS_2 Anode for Rechargeable Lithium Battery. *J. Power Sources* **2001**, *97−98*, 198–200.
29. Zai, J. T.; Wang, K. X.; Su, Y. Z.; Qian, X. F.; Chen, J. S. High Stability and Superior Rate Capability of Three-Dimensional Hierarchical SnS_2 Microspheres as Anode Material in Lithium Ion Batteries. *J. Power Sources* **2011**, *196*, 3650–3654.
30. Kang, J. G.; Park, J. G.; Kim, D. W. Superior Rate Capabilities of SnS Nanosheet Electrodes for Li Ion Batteries. *Electrochem. Commun.* **2010**, *12*, 307–310.
31. Seo, J. W.; Jang, J. T.; Park, S. W.; Kim, C. J.; Park, B.; Cheon, J. Two-Dimensional SnS_2 Nanoplates with Extraordinary High Discharge Capacity for Lithium Ion Batteries. *Adv. Mater.* **2008**, *20*, 4269–4273.
32. Wang, Y.; Lee, J. Y. One-Step, Confined Growth of Bimetallic Tin−Antimony Nanorods in Carbon Nanotubes Grown *in Situ* for Reversible Li^+ Ion Storage. *Angew. Chem., Int. Ed.* **2006**, *45*, 7039–7042.
33. Li, R. Y.; Sun, X. C.; Zhou, X. R.; Cai, M.; Sun, X. Aligned Heterostructures of Single-Crystalline Tin Nanowires Encapsulated in Amorphous Carbon Nanotubes. *J. Phys. Chem. C* **2007**, *111*, 9130–9135.
34. Kumar, T. P.; Ramesh, R.; Lin, Y. Y.; Fey, G. T. K. Tin-Filled Carbon Nanotubes as Insertion Anode Materials for Lithium-Ion Batteries. *Electrochem. Commun.* **2004**, *6*, 520–525.
35. Razak, S. I. A.; Ahmad, A. L.; Zein, S. H.; Boccaccini, A. R. MnO_2-Filled Multiwalled Carbon Nanotube/Polyaniline Nanocomposites with Enhanced Interfacial Interaction and Electronic Properties. *Scr. Mater.* **2009**, *61*, 592–595.
36. Yu, Y.; Gu, L.; Wang, C.; Dhanabalan, A.; van Aken, P. A.; Maier, J. Encapsulation of Sn@Carbon Nanoparticles in Bamboo-like Hollow Carbon Nanofibers as an Anode Material in Lithium-Based Batteries. *Angew. Chem., Int. Ed.* **2009**, *48*, 6485–6489.
37. Hassoun, J.; Derrien, G.; Panero, S.; Scrosati, B. A Nanostructured Sn−C Composite Lithium Battery Electrode with Unique Stability and High Electrochemical Performance. *Adv. Mater.* **2008**, *20*, 3169–3175.
38. Ng, M. F.; Zheng, J. W.; Wu, P. Evaluation of Sn Nanowire Encapsulated Carbon Nanotube for a Li-Ion Battery Anode by DFT Calculations. *J. Phys. Chem. C* **2010**, *114*, 8542–8545.